Measurement Instrument Selection for Very High Bit Rate Contactless Transponder Evaluation

David Seebacher
Student, TU Graz
Graz, Austria
david.seebacher@student.tugraz.at

Michael Gebhart, Michael Stark
RF Systems
NXP Semiconductors
Gratkorn, Austria
gebhart@ieee.org, michael.stark@nxp.com

Abstract— **In this paper we discuss properties of the digital sampling oscilloscope versus signal analyzer as instrument in the test bench to characterize ISO/IEC14443 compliant contactless communication devices. An extension to the existing near-field communication (NFC) standard specifies very high bit rates (VHBR) in the range of 10 Mbit/s for the Reader to Transponder communication link. One draft specification takes advantage of sophisticated signal processing and clever coding, to allow an energy-efficient contactless system, compliant to existing frequency regulation and to typical Reader hardware, which can also be used in mobile applications such as NFC in Smartphones. Considerations for the test bench to characterize this communication air interface are of general interest also for existing RFID standards in the 13.56 MHz frequency band.**

I. INTRODUCTION

Like for all communication interfaces, the interoperability of products from different manufacturers to the specifications described in an International Standard is the key for practical applicability and commercial success. Casual consideration would indicate that requirements to the measurement instrumentation for contactless near-field communication technologies in the 13.56 MHz frequency band are comparatively simple, because challenges of an RF interface, which typically is in the GHz frequency domain today, would scale down with the low operating frequency, which is well understood since the 1930ies. And so almost any measurement instrument, developed mainly with focus on signal analysis in the GHz domain today could also well be used in a contactless test bench, if only the specified low cut-off frequency would allow this.

As specialists in development and characterization of such contactless products as electronic Passports, contactless Smartcards and tickets, we find this a very shallow view in practice, although even some communication professionals still share this opinion. It does not reflect reality, as two aspects seem to be forgotten: First, it is a battery-less technology, which means a major extension in requirements as compared to any conventional wireless communication interface and brings also a shift in priority of aspects to be considered, and second, integrated semiconductor processor technology and all related aspects on equivalent circuit and air interface have *not* been existing and investigated in the 1930ies.

The development of a new very high bit rate (VHBR) communication interface as an amendment to the proximity standard ISO/IEC 14443 [1] was the trigger for this investigation on appropriate measurement instrumentation. For this sophisticated approach on 13.56 MHz carrier, the challenges for the measurement equipment are even more distinct, although the same aspects must be considered also for todays standard air interface ISO/IEC14443 type A and type B [2], which specifies data rates up to 847.5 kbit/s. At this time, for Reader to Transponder communication there are 2 alternative options for the VHBR interface specifications: Amplitude Shift Keying (ASK) with similar specifications as 14443B, reducing the bit duration in 3 steps by a factor of 2 for bit rates up to 6.78 Mbit/s, and multiple Phase Shift Keying (mPSKn) with an information content of m = 1 – 4 bits per symbol, theoretically allowing data rates up to 13.56 Mbit/s, in practice to date achieving up to 6.78 Mbit/s as functional blocks integrated on silicon. The defined matrix for data rates is given in tab. I.

TABLE I. ACHIEVABLE VHBR DATA RATES

symbol duration (n)	ASK	2PSKn	4PSKn	8PSKn	16PSKn
cycles (τ_C)	*Mbit/s*				
16	(0.848)	-	1.695	2.542	3.39
8	1.695	1.695	3.39	5.09	6.78
4	3.39	3.39	6.78	10.17	-
2	6.78	6.78	13.56	-	-

It should be added, all ASK VHBR options and some mPSKn VHBR options can be considered as Ultra Wide Band (UWB) as defined by the Federal Communications Commission (FCC), according to their spectral emission to transmit the information as they have a modulation bandwidth which exceeds 20 % of the carrier frequency [3]. Some mPSK options, e.g. for n = 16, are conformant with the existing spectral emission mask in EN 300330 [4]. This aids the argumentation for a good choice of instruments to characterize such components, and will also require the introduction of a new frequency regulation for the data rates which are concerned (all ASK and some mPSKn VHBR options).

The contactless test bench consists of signal generation, an antenna arrangement with specified parameters for the air interface according to the proximity card test standard

ISO/IEC10373-6, and an analyzer instrument, which can be a vector signal analyzer, or an oscilloscope in principle. In this paper we investigate, which measurement concept for signal analysis is most appropriate. Also for the test standard this is a valid question, as it was discussed some time ago in the working group to replace the term "*digital oscilloscope*" by a more general term "*digital sampling instrument*", which would also allow a signal analyzer for all measurements. However, the latest revision of 2011 specifies an oscilloscope. For the data format mPSK, the vector signal analyzer seems to be the logical choice at the first thought, as it is intended to display signals in the constellation plot. However, can this feeling be verified by hard facts? A broadband data stream is transmitted over an exceptional low carrier frequency of 13.56 MHz, which is a good choice from energy transmission perspective. Settling time effects become important out of this reason. Moreover, typical spectrum and vector signal analyzers are constructed in a way that they are best suited for RF signals above a certain intermediate frequency (IF), e.g. 100 MHz, at which the signal is sampled. However, all major measurement instrument manufacturers in the meantime offer both, oscilloscopes and analyzers, so we can highlight pros and cons for each concept in the context of contactless technologies, without harming the interests of an individual instrument manufacturer.

II. Specification of PSK VHBR Reader to Card Communication Interface

The aim of the development of PSK based contactless transmission system was to use sophisticated signal processing to achieve an energy-efficient system. This also allows mobile applications like the upcoming NFC, based on typical contactless reader using a single antenna of a resonance circuit with an operational Q-factor around 15.

Data is transmitted in frames of defined length up to 4 kBytes, consisting of a header and payload data, protected by several error recognition and correction techniques.

A transponder usually has no own absolute time reference but recovers the clock from the 13.56 MHz carrier – the base standard specifies all relevant timing in carrier periods $\tau_C = 1/f_C$ out of this reason. The VHBR mPSKn interface specifies differential coding, so the transponder just needs to detect a symbol relative to its preceeding symbol, which can be achieved with an integrated Phase Locked Loop (PLL) as relative phase reference. As a higher order modulation format is used, one symbol may encode several bits of information. Gray coding is used to guarantee that one symbol error (which most probably means that a neighbor symbol is detected instead of the correct one) will result in one single bit error only. Hamming code allows to detect 2 bit errors and to correct one, furthermore CRC 32 protects the complete frame.

The modulation options to achieve data rates of up to 13.56 Mbit/s for the Reader to Card communication direction are given in tab. I. The modulation is specified as mPSKn, where m denotes the modulation order, the number of symbols in the alphabet, and n gives the symbol duration in carrier cycles. The transition between symbols (e.g. any cosine roll-off factor) is not specified, so we will consider immediate symbol transitions here. To provide sufficient energy in the carrier frequency for contactless power transmission to the Smartcard chip, and to keep the emission limits low in the modulation bandwidth, which is usually the limiting factor for small Reader antenna systems, only a part out of the full 360 ° phase state plane is used for modulation [5]. This part is referred as *IQ segment*, specified to 60 ° or π/3.

In Fig. 1 constellation diagrams for all specified modulation options are plotted. As an example, for 2PSKn the alphabet consists of only 2 symbols, each representing an information content of 1 bit. Consequently the symbol interval is specified equal to the full IQ segment of 60 ° with two ideal symbol phase states at 0 ° and 60 ° relative to the carrier in the constellation diagram. This constellation diagram is shown on the top left corner of Fig. 1. In the top right corner the constellation diagram of the 4PSK is visualized showing a minimum angle of –20 ° and a maximum angle of 40 °, resulting in a symbol interval of 20 °. The constellation diagram of the 8PSK signal is shown in the bottom left corner. It has a symbol interval of 8 ° and a minimum and maximum modulation angle of –24 °and 32 °, respectively. The 16PSK modulation has a symbol interval of only 4 °, which results in constellation points ranging from –28 ° to 32 °. This can be seen in the bottom right corner.

Not all combinations of modulation orders and symbol durations are defined. The 2PSK2 combination is not used as with a data rate of 848 kbit/s it is equal to the maximum data rate already defined in the existing standard for ASK. The 8PSK2, 16PSK4 and 16PSK2 combinations are also not defined. So 4PSK2 offers with 13.56 Mbit/s the highest data rate. It was also found that this is the most critical constellation to measure.

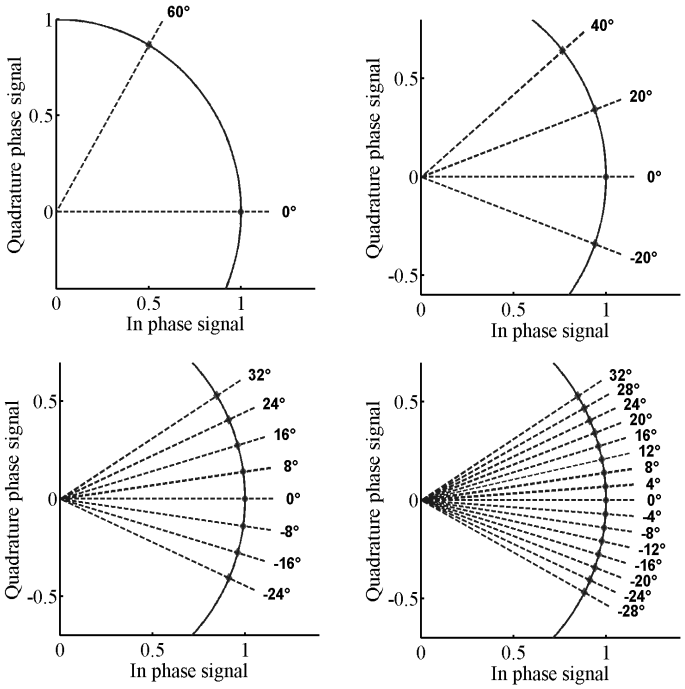

Figure 1. Constellation diagrams showing IQ segment and symbol positions of 2PSK, 4PSK, 8PSK and 16PSK (top left to bottom right), taken from [1].

For the generation of the signal an arbitrary waveform generator specifically developed by NXP[1] for the operation at 13.56MHz with low noise properties was used [6]. As this instrument was tailored specifically for operation at the carrier frequency, a harmonic mode crystal is used instead of a fractional PLL, which usually provides the frequency reference of conventional general purpose commercial instruments. In tab. II the structure of a VHBR frame can be seen. It consists of a start of frame (SOF) and data. The SOF includes a calibration sequence (CAL) of 44 symbols, a synchronization sequence (SYNC) of 4 symbols and a training sequence (TSC) with a length of 92 symbols. The calibration sequence consists of 2 consecutive symbols alternating between two constellation points. The synchronization sequence uses the same constellation points as the calibration sequence but each symbol alternates. The training sequence consists of pseudo random symbols.

TABLE II. VHBR FRAME

CAL	SYNC	TSC	DATA
44 symb.	4symb.	92 symb.	N symb.

The data can have a size of up to 4 kBytes which results in different symbol lengths according to the modulation order.

III. SIGNAL ANALYSIS

The intended modulation concept results in very small PSK symbol interval angles. Consequently this results in very stringent phase noise requirements for signal generation and analysis in the test bench. Moreover, the noise floor of the analysis instrument should be below the noise floor of the signal generator so that the main amount of noise is not added during analysis, distorting the measurement result.

Another important criterion for the selection of the analysis instrument is to avoid inter-symbol interference (ISI) generation in the signal analysis path. This is to guarantee to measure the authentic signal present at the air interface, avoiding any influence of the measurement instrument. The capabilities of two state of the art vector signal analyzers and one state of the art digital sampling oscilloscope to analyze the given mPSKn signals have been tested. In the subsequent sections the different properties of the spectrum analyzer and the oscilloscope are compared. All measurements presented in this paper were done with a cable connection between the generator and the analyzer including a proper 50 Ω termination, instead of the antenna air interface. The cable connection was used to measure the signal quality, comprising the generation and analysis and excluding the influence of the transmission channel. Although the final use case is the analysis of signals present at the air interface of the contactless test bench. For the tests performed frames containing the SOF followed by 256 random symbols were used.

A. *Signal processing chain*

Signal analyzer and oscilloscope have two different operating principles. For the measurements performed both instruments were used to acquire time series of discrete amplitude values. After data acquisition these time series for in-phase (I) and quadrature phase (Q) are corrected and analyzed offline in a MATLAB[2] signal processing chain on a personal computer (PC), which is equal for both instruments.

Signal analyzers are designed to capture and analyze signals in the spectral domain. They operate from almost DC up to several GHz offering a certain analysis bandwidth, e.g. 40 MHz. In order to cover this large frequency range the input signal is mixed with the local oscillator (LO) of the analyzer. In Fig. 2 the signal processing chain of a typical analyzer can be seen. The RF signal at 13.56 MHz passes one or more intermediate frequency (IF) stages, being mixed up before reaching the final IF, e.g. at 96 MHz. Before performing IF sampling e.g. with 128 MHz sampling rate, the input signal passes a band-pass (BP) filter, e.g. of 40 MHz. The transfer function of this analog filter is compensated in the digital domain by an equalizer. After this compensation the IQ-demodulation using a numerically controlled oscillator (NCO) is performed. The resulting IQ-samples are then low-pass filtered and resampled to the desired target sampling rate. Then they are stored in the instruments memory from where they are accessible over an interface for further PC-based offline signal processing. Due to this instrument principle, the original time series is not accessible.

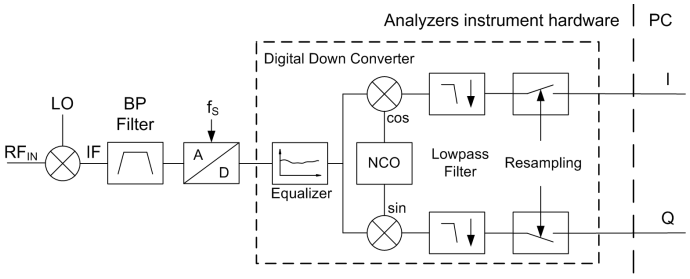

Figure 2. Signal processing chain of the signal analyzer, modified [9].

An *oscilloscope* is designed to capture and analyze signals in time domain. The amplitude resolution may be minor to a spectrum analyzer, offering e.g. 8 bit amplitude resolution per sample, but modern digital sampling scopes allow sampling rates up to the GS/s domain. This option can be used to convert margin in time resolution to higher amplitude resolution, according to [7] and [8]. The theoretically possible gain can be calculated by (1), where ΔRES denotes the gain of resolution in bits and OSR is the oversampling ratio with respect to the Nyquist frequency limit for the information signal bandwidth.

$$\Delta RES = \frac{1}{2} \cdot \log 2(OSR) \tag{1}$$

[1] www.nxp.com

[2] www.mathworks.com

Figure 3 shows a typical signal processing chain for a digital scope. The captured time series is directly accessible from the instrument and can be processed further and offline on a PC, e.g. using MATLAB.

In detail, for the instrument we have used, the RF signal captured at a 50 Ω terminated input passes the anti-aliasing filter (AAF) before being directly sampled with a sampling rate of f_S = 2.5 GS/s. After the sampling a low-pass filter (LP) with a cut-off frequency of 72.5 MHz available on the oscilloscope was used, to enhance the amplitude resolution by 2 bits and to remove the out of band noise produced by the instrument. This time-series data, stored in the instrument memory, is then accessible over an interface for PC based signal processing, implemented in MATLAB. This includes the IQ-demodulation with subsequent low-pass filtering and resampling to a lower sampling rate.

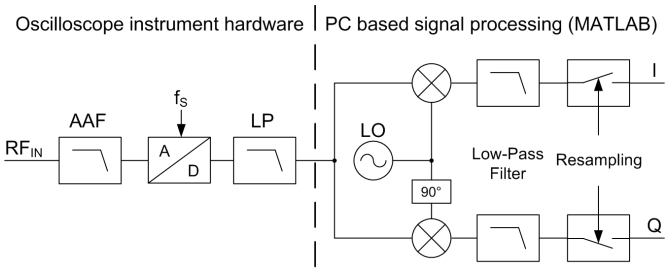

Figure 3. Signal processing chain of the digital sampling oscilloscope.

Before signal analysis, both time-discrete *I* and *Q* channel signals of Fig. 2 or 3 pass a correction chain shown in Fig. 4, which is also implemented in MATLAB. If the local oscillator of the RF signal generator and the analyzer instrument are not phase-locked, their frequencies slightly differ, which leads to a frequency error. To correct this error the difference has to be estimated. For typical scopes it is not possible to lock the internal LO to the generator. Spectrum analyzers usually support this option, but for offline processing no significant difference between the synchronized and the free running mode was observed for the short signal observation period of a few milliseconds.

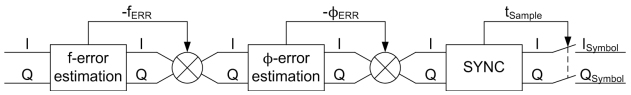

Figure 4. Measurement error correction signal processing chain, implemented in MATLAB.

In the 1st step, the *frequency error* is estimated using the unmodulated carrier before the transmitted frame. If there is a frequency error in the signal, the phase shows a linear increase or decrease over time. The slope and accordingly the frequency error of this trace is determined by a first order polynomial fit. The estimated frequency error is used to correct the IQ time series by mixing with the negative frequency error.

In the 2nd step, the *phase error* is estimated by the mean value of the frequency corrected unmodulated carrier's phase. The phase error is corrected by a complex mixing process rotating the IQ-plane by the measured phase error. After this step, the unmodulated carrier corresponds to an angle of zero degree in the IQ-plane. These two steps emulate the behavior of a PLL which locks to the carrier and is in free running mode during the reception of the frame.

The last step is the recovery of the *symbol timing* which is done by correlating received to transmitted data. The sampling time was set to the middle of the symbol grid for the final sampling of the IQ-values of one symbol. The effects of a different sampling position are covered in the subsequent section. For the analyzer only 3 samples per symbol for the shortest symbol duration (2 carrier cycles) are available, which means that the synchronization block can choose among only 3 samples. Therefore the signal was upsampled before doing the synchronization in order to find the best sample position. It was found that this gives a better performance for signals with short symbol duration. The symbols are then used to analyze the quality of the signal regarding phase noise and their position in the IQ-plane.

B. Analysis bandwidth

The analysis bandwidth has a major influence on the noise as well as on signal transitions. The absolute noise power increases with the equivalent bandwidth used for signal analysis. The higher the analysis bandwidth is, the higher the noise gets. Using a narrow band filter, e.g. a raised cosine filter, to increase the signal to noise ratio (SNR) is no option, as the signal present at the air interface has to be verified and no additional distortion shall be added during analysis.

A main limitation for the signal analyzer is the narrow analysis bandwidth due to its operational principle and the low carrier frequency. The mixing process is done in the analog domain with all its non ideal properties. In fig. 5 the unmodulated carrier at 13.56 MHz can be seen in the center of the spectrum.

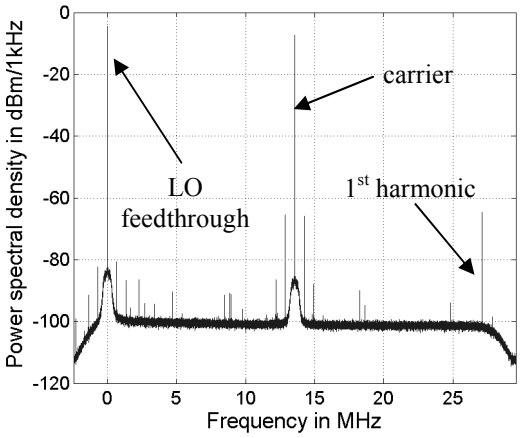

Figure 5. Spectrum carrier measured with analyzer.

Beside the carrier there is also the LO-feed-through at DC and the first harmonic at 27.12 MHz visible. This limits the analysis bandwidth to less than 27.12 MHz. A sampling rate of f_S = *20.34 MHz (1.5* f_C*)* was empirically found to be a good trade off to avoid the influence of those two frequency components and still to have an acceptable analysis bandwidth. The resulting bandwidth is *0.8* f_S which is 16.27 MHz for a sampling rate of *1.5* f_C [9].

The oscilloscope directly samples the signal and the mixing process is performed in the digital domain under ideal conditions. Therefore no LO-feed-through at DC exists. The limitation for the oscilloscopes bandwidth is the negative carrier at -27.12 MHz (after the IQ-demodulation). For filtering the demodulated signal of the oscilloscope a mean filter with the length of one carrier period was used. This filter has a bandwidth of 12.07 MHz between its -3dB points and noise bandwidth of 13.56 MHz. The equivalent noise bandwidth is defined as the bandwidth of an ideal rectangular filter, which allows the same amount of white noise power to pass as the original filter [10]. The mean filter has a zero in its transfer function exactly at 13.56 MHz and all multiples of it, which removes all the undesired frequency components.

In Fig. 6 shows the transfer function of the mean filter used for the oscilloscopes data and a low-pass-filter design similar to the filter which is used in the analyzer. These filters are also used for the simulations described in chapter V.

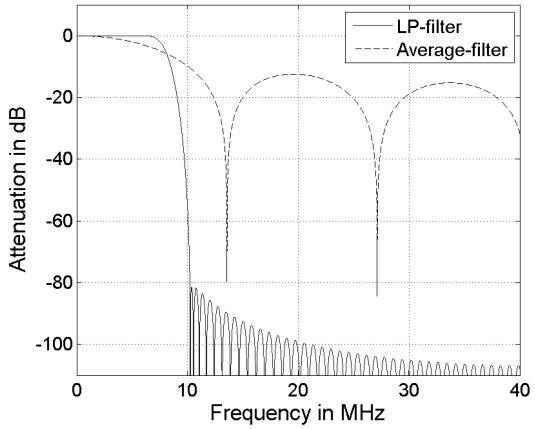

Figure 6. Low-pass-filters spectral transfer function.

IV. MEASUREMENT RESULTS

In this section the measurement results will be presented and discussed. This includes the analysis in the time domain, as well as the influence of the sampling position and the phase noise. Finally the measurement results are visualized in the constellation diagram, which gives a good overview about ISI contained in the signal.

A. Phase signal in time domain

In Fig. 7 and Fig. 8 the time traces of the demodulated phase signal are plotted for both instruments. The figures show a part of the frame containing the last 4 symbols of the calibration sequence, the sync sequence and the start of the training sequence.

The signal captured with the analyzer is given in Fig. 7. It can be seen that the signal shows ringing after each symbol transition. This is due to the band-limitation by the very steep filter (Gibbs phenomenon [11]). The ringing needs more than 8 carrier cycles to fully decay, which is already one symbol duration for the 16PSK8 modulation. This influences the symbol recognition significantly. The effects will be covered in the following section more in detail. The same signal captured with the oscilloscope is plotted in Fig. 8. The signal does not show any overshoots or suffers from ringing at all. This is due to the larger analysis bandwidth and the more relaxed filter design.

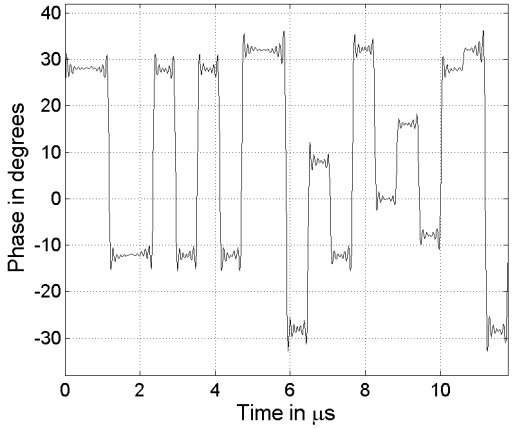

Figure 7. 16PSK8 communication sequence captured with analyzer.

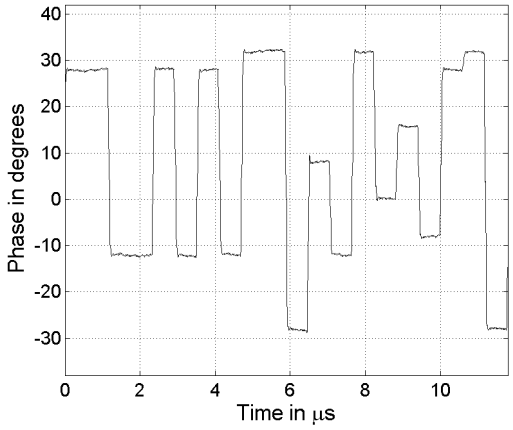

Figure 8. 16PSK8 communication sequence captured with scope.

B. Influence of the sampling position

It was found that the selection of the symbol sampling position has a severe influence on the symbol phase noise in the constellation plot. Fig. 9 depicts the influence of the sampling position for the analyzer. The analysis shown in this figure was done for a 4PSK signal with different symbol durations. On the x-axis the relative sampling position with respect to the symbol grid is plotted. The y-axis gives the root mean square (RMS) phase error of the symbols. It can be seen that the RMS phase error is influenced by the ringing effects which are described in section A. The longer the symbol duration is, the longer the ringing has time to decay. The 4PSK2 signal, representing the shortest symbol duration shows the largest symbol phase error as the symbol is sampled at very incomplete phase signal settlings. The 4PSK16 representing the longest symbol duration shows the least symbol phase error and the best performance as the ringing is almost fully decayed until the middle of the symbol duration. If the symbol is sampled at the beginning or the end of the symbol grid, the symbol phase error is largest, as there is a very steep phase transition close to the edges of the signal. The ringing effect

dominates, with the lowest influence in the middle of the symbol grid. For the longest symbol duration of 16 carrier cycles the phase noise already is the main component of the symbol phase error.

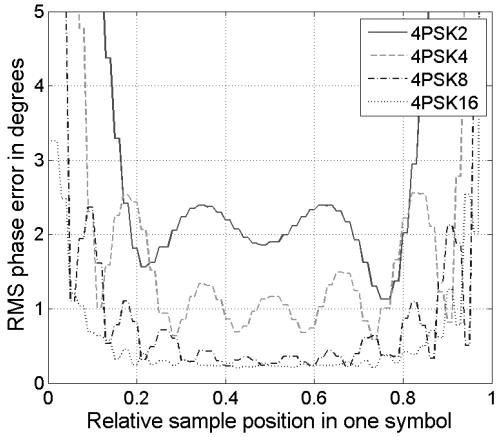

Figure 9. Phase error vs. sampling position for the analyzer.

In Fig. 10 the same analysis is shown for the oscilloscope. The RMS symbol phase error of the oscilloscope increases as well close to the boarders of the symbol grid, but it settles much faster than the signal captured with the analyzer, due to the higher bandwidth. The settling time is constant and independent of the symbol rate. If the symbol duration is increased by a factor of two, the relative settling time decreases by a factor of two as well. Even for the shortest symbol duration (4PSK2) the signal has settled until the middle of the symbol grid and what remains is the phase noise.

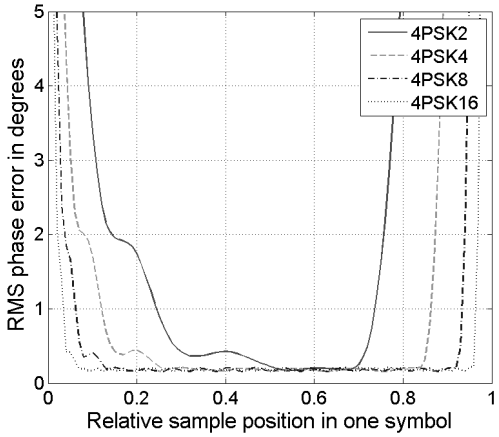

Figure 10. Phase error vs. sampling position for the oscilloscope.

As for the analyzers the middle of the symbol durations shows the lowest error and as for oscilloscope the signal is settled under all conditions at this point, the signal was sampled at the middle of the symbol grid for further analysis.

C. Phase noise

The phase noise is one of the main limiting factors of the measurement accuracy. Therefore the phase noise of the unmodulated carrier was analyzed, which also gives the lower bound of the phase noise for the analysis of the modulated signal. As the used generator has a very low noise floor, the Displayed Average Noise Level (DANL) [10] of the measurement instrument is of importance.

For the measurements performed with the analyzers the reference plane was set to 0 dBm using an internal attenuator of 10 dB, which results a DANL of -142 dBm/Hz, respectively -141 dBm/Hz [12] and [13].

For the oscilloscope the measured noise floor was at -99.16 dBm/5kHz and can be converted into a resolution bandwidth of 1 Hz by using (2) according to [10]. Where ΔDANL denotes the change of the noise floor in dB and $B_{R,ZF1}$ and $B_{R,ZRF2}$ are the equivalent noise bandwidth before and after the conversion. Performing this conversion for the with 5 kHz noise bandwidth measured noise floor of the oscilloscope to a resolution bandwidth of 1 Hz requires a correction by -36.99 dB, which yields a DANL of -136.15 dBm/Hz.

$$\Delta DANL = 10 \cdot \log 10\left(\frac{B_{R,ZF2}}{B_{R,ZF1}}\right) \tag{2}$$

The corresponding reference level using an amplitude resolution of 50 mV/Div and 8 divisions vertical resolution was -3.97 dBm, assuming a sine wave signal over the full resolution of the analog to digital converter (ADC).

A measurement of the noise floor of the signal generator can be seen in Fig. 5, where the noise floor is at -100.85 dBm/1kHz. Converting this value according to (2) to a resolution bandwidth of 1 Hz gives -130.85 dBm/Hz.

The DANL of the signal analyzer, with which the noise floor signal generator was measured, as well as the one of the oscilloscope, are already close to the measured signal. The measured signal consists of the noise power of the signal generator plus the internal noise power of the signal analyzer, which results in a difference of the measured value as can be calculated with (3) according to [10].

$$\Delta MEAS = 10 \cdot \log 10\left(\frac{S + DANL}{S}\right) \tag{3}$$

The difference ΔMEAS of the measured signal in dB depends on the ratio of the signal power plus the noise power of the analyzer (DANL) to the signal power itself. The signal power can be calculated by subtracting the DANL from the measured value in the linear domain. Correcting the measured noise floor yields -131.2 dBm/Hz. This corresponds to an offset of 0.35 dB, respectively 0.43 dB for the analyzers and already 1.2 dB for the oscilloscope.

In Fig. 11 the spectrum of the phase noise for one analyzer and the oscilloscope is plotted. The influence of the different filters can be seen. The analyzers phase noise floor decreases rapidly above the cut-off frequency of its analysis filter at 8.14 MHz, whereas the phase noise floor measured with the oscilloscopes follows the transfer function of the mean filter.

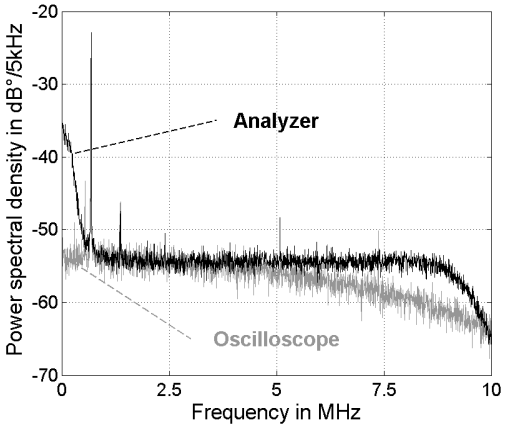

Figure 11. Phase noise spectrum comparison.

A spike at 672 kHz is due to spurious emissions of the signal generator. The phase noise of the analyzer significantly increases towards zero. This is due to the phase noise of the LO, which is added to the signal during the mixing process.

The RMS phase noise (Φ_{RMS}) is evaluated by calculating the RMS value of the difference between the measured and the ideal (reference) signal (4). Where Φ_{MEAS} is the measured phase and Φ_{REF} denotes the phase of the reference (transmitted) signal. N corresponds to the number of samples and n is the running index over them.

$$\Phi_{RMS} = \sqrt{\frac{1}{N}\sum_{n=0}^{N-1}\left(\Phi_{MEAS}[n]-\Phi_{REF}[n]\right)^2} \qquad (4)$$

Evaluating equ. (4) for the unmodulated carrier gives the RMS phase noise without any influence of ISI. An RMS phase noise of 0.224 ° for a bandwidth of 16.28 MHz was measured with the signal analyzer. The measurement with the oscilloscope delivered an RMS phase error of 0.175 ° for an equivalent noise bandwidth of 13.56 MHz. The measured values are different due to the difference in the analysis bandwidth used, the larger the bandwidth, the larger the noise.

Both measurement instruments contribute to the measured phase noise to a certain amount. This increase is still acceptable, but not negligible. If very accurate results are required the measured data has to be corrected (3) by the measurement instrument contribution to the phase error.

D. Constellation diagrams

Analyzing the signal in the constellation diagram gives a nice overview. For longer symbol durations no significant difference between the oscilloscopes' and the analyzers' result were observed. For shorter symbol durations differences due to the narrow band filtering in the analyzer's signal processing chain were observed.

In Fig. 12 the constellation diagram of a 4PSK2 frame recorded with the analyzer is plotted. The real part corresponds to the x-axis and the imaginary part to the y-axis. It can be seen that the constellation diagram suffers from ISI (increased due to the ringing). The RMS phase error is 1.95 °, which includes also the effects of ISI and not only the phase noise. The maximum phase error is 4.79 °.

The measurement results of the oscilloscope are shown in Fig. 13. It can be seen that the measured constellation points to correspond quite well to the sent ones. The RMS phase error of 0.23 ° is significantly lower than the RMS phase error of the analyzer.

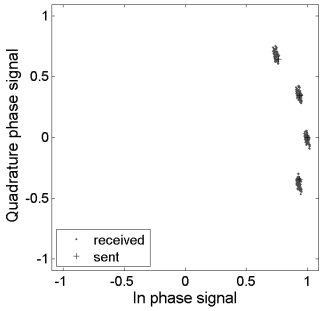

Figure 12. 4PSK2 constellation diagram measured with analyzer.

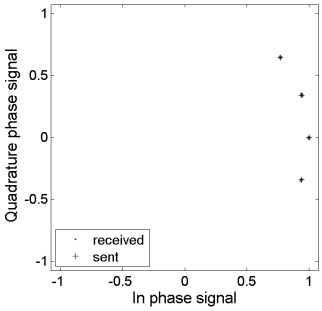

Figure 13. 4PSK2 constellation diagram measured with oscilloscope.

Tab. III summarizes the RMS phase error measured for the 4PSKn signal and different symbol durations for both instruments.

TABLE III. 4PSKN $\Phi_{ERR\ RMS}$

symbol duration	**Analyzer**	**Oscilloscope**
τ_C	degrees	degrees
16	0.226	0.174
8	0.270	0.175
4	1.190	0.179
2	1.947	0.231

The RMS phase error of the analyzer depends heavily on the symbol duration due to the ringing effect. For the longest symbol duration of $n = 16\ \tau_C$ it approaches with 0.226 ° the value of the pure RMS phase noise of 0.224 °, but the shorter the symbol gets the larger the RMS phase error gets as well.

The results of the oscilloscope show only a slight increase of the phase error for the shortest symbol duration of $n = 2\ \tau_C$ as it does not suffer significantly from the ringing effect.

These tendencies are valid for all different modulation orders and different measurement scenarios.

V. SIMULATION RESULTS

To confirm the measurement results and to understand the influence of the band-limitation additional simulations were performed. The low-pass filter design plotted in Fig. 6 is used for the simulation of the analyzer, whereas the mean filter design is used to simulate the behavior of the oscilloscope's signal processing chain. In Fig. 14 the results of simulating a 16PSK8 frame containing the same data as in Fig. 7 is shown. It can be seen that the signal also contains overshoots and suffers from ringing.

The results of using the mean filter of the oscilloscope are shown in Fig. 15. As for the measurement results the signal does not show any overshoots nor suffers from ringing at all.

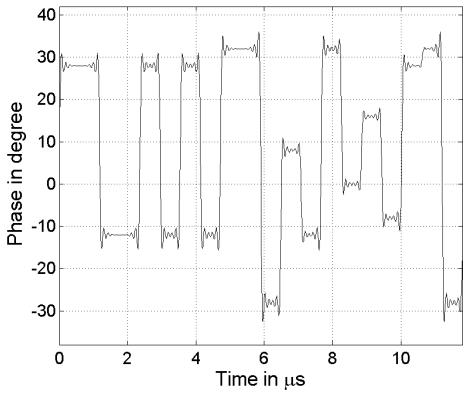

Figure 14. 16PSK8 time domain low-pass filtered, simulated.

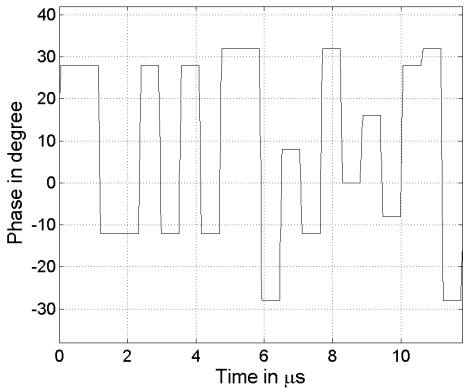

Figure 15. 16PSK8 time domain mean filtered, simulated.

The simulation results confirm the root causes for the effects observed in the measurements. It can be concluded that limiting the analysis bandwidth with a very steep filter has negative influence on the signals transient's behavior and might introduce additional error.

VI. CONCLUSION

The properties of two state of the art signal analyzers and one digital sampling oscilloscope in the content of the analysis of a mPSKn signal on a 13.56 MHz carrier according to [1] have been analyzed. The basic operational principles and the used signal processing chains have been outlined. The differences between the two signal processing chains have been pointed out. The measurement results have been analyzed in various ways to provide a complete picture of the properties. Additionally simulations have been performed to confirm the effects of different filtering options.

The signal analyzers offer the possibility to synchronize to the generator, but as the frequency offset can be corrected numerically, it was found that this is not necessary. The DANL of both instruments has an influence on the measured signal, where the analyzers show better values. But on the other hand the signal analyzers introduce additional phase noise of their LO through their operational principle involving analog mixing.

The signal analyzers also suffer from their limited bandwidth when analyzing broadband signals with short symbol durations. The oscilloscope on the other hand offers a greater analysis bandwidth. The possibility of using a higher analysis bandwidth for the signal analyzers and removing the LO-feed-through at DC by a notch filter was not tested and could be a possibility to improve the performance of the analyzers.

The oscilloscope was selected as the preferred measurement instrument, because the whole signal processing can be influenced, the analysis bandwidth is not limited by the LO-feed-through at DC and it is already used in many test benches.

ACKNOWLEDGMENT

The authors wish to acknowledge the support of the Oesterreichische Forschungsförderungsgesellschaft (FFG). The work presented in this paper is part of the VHD project, with the aim to enhance data rates for NFC, which is partly funded by FFG and NXP [14].

REFERENCES

[1] ISO/IEC 14443-3:2010/PDAM 2: Identification cards — Contactless integrated circuit cards — Proximity cards — Part 3: Initialization and anticollision: Amendment 2 Bit rates higher than fc/16 up to fc and increased frame size, Nov. 2010.

[2] ISO/IEC 14443-2: Identification cards — Contactless integrated circuit cards — Proximity cards — Part 2: Radio frequency power and signal interface, 2nd edition, Sept. 2010.

[3] FCC Code of federal regulation, 47 CFR, Part 15- Radio Frequency Devices, 2010

[4] ETSI EN 300 330-1: Electromagnetic compatibility and Radio spectrum Matters (ERM); Short Range Devices (SRD); Radio equipment in the frequency range 9 kHz to 25 MHz and inductive loop systems; Part 1: Technical characteristics and test methods, version V1.5.1, Jan. 2006

[5] Gossar, M., Stark, M., Gebhart, M., Pribyl, W. and Soser, P., Investigations to achieve very high data Rates for proximity coupling devices at 13.56 MHz and NFC applications, 3rd International Workshop on Near Field Communication (NFC), Feb. 2011, pp.71-76.

[6] M. Gebhart, S. Birnstingl, J. Bruckbauer, E. Merlin, "Properties of a test bench to verify Standard Compliance of Proximity Transponders", in CSNDSP, July 2008, pp. 306-310.

[7] Lecroy, Application Note A006A: Enhanced Resolution

[8] STMicroelectronics, Application note AN2668: Improving STM32F101xx and STM32F103xx ADC resolution by oversampling, 1st edition, July 2008

[9] Rohde&Schwarz. R&S FSV-K70 Firmware Option Vector Signal Analysis Operating Manual, 2010.

[10] Rauscher, C., Janseen, V.; Minihold R., Grundlagen der Spektrumanalyse, R&S GmbH, 1st edition, 2000

[11] A.V. Oppenheim, and R.W. Schafer, "Discrete-Time Signal Processing", Prentice-Hall, Englewood Cliffs, NJ, 1989

[12] Rohde&Schwarz. R&S FSV Signal and Spectrum Analyzer Specifications, Feb. 2010.

[13] Agilent. N9020A MXA X-Series Signal Analyzer Data Sheet, Dec. 2010.

[14] H. Witschnig, VHD-High Speed-Air Interface and IC-Architecture for Contactless Smartcards and NFC, FFG FIT-IT Call 4, June 2008